A Comparative Study of Nitrogen Physisorption on Different C_{70} Crystal Structures Using an Ab Initio Based Potential

Gaurav Arora,[†] Jeffery B. Klauda,[‡] and Stanley I. Sandler*[,†]

Center for Molecular and Engineering Thermodynamics, Department of Chemical Engineering, University of Delaware, Newark, Delaware 19716, and Laboratory of Computational Biology, National Institutes of Health, National Heart, Lung, and Blood Institute, Building 50, 50 South Drive, Bethesda, Maryland 20892

Received: February 2, 2005; In Final Form: May 10, 2005

Quantum mechanical calculations are performed using the recently developed hybrid method for interaction energies to determine atom site Lennard−Jones potential parameters for the interactions of molecular nitrogen with C_{70} molecules. This ab initio based potential is used in grand canonical Monte Carlo simulations to predict surface adsorption properties of N_2 on five known C_{70} structures: rhombohedral, fcc, ideal hcp, deformed hcp, and monoclinic crystals. Because of the presence of five-membered carbon rings and the surface curvature of C_{70} molecule, the Lennard−Jones potential parameters for nitrogen−carbon interactions obtained from ab initio based calculations are found to be different from that with planar graphite. The simulation results obtained from these two sets of force fields are compared and shown to differ, particularly at low coverage, where the nitrogen−carbon interactions are more important than the nitrogen−nitrogen interactions. The surface area, monolayer capacity, and isosteric heat of adsorption are calculated for various C_{70} crystals and found to change appreciably as a result of the shear-induced phase transformation from hcp to rhombohedral lattice.

I. Introduction

Since the production of fullerenes in macroscopic quantities have become possible,[1,2] fullerenes have been of research interest in diverse fields of chemical science, physics, and material science. Fullerene molecules, C_{60} and C_{70}, form the main components of fullerite soot and are known to have remarkable electronic and magnetic properties[3,4] and have possible applications in a variety of areas such as enzyme inhibition,[5] antiviral agents,[5] photoconductive materials,[6,7] and gas separation membranes.[8]

In the solid phase, various crystal forms of C_{60} and C_{70} have been determined experimentally,[9−13] and there have been experimental and simulation studies for gas adsorption on C_{60} and C_{60}/C_{70} fullerene crystals.[14−18] Martinez-Alonso et al.[15] studied the surface properties of C_{60} fullerene by means of Ar, CO_2, and N_2 adsorption by both experiment and grand canonical Monte Carlo (GCMC) simulation and found higher affinity of the adsorbent on these surfaces than on a planar graphite sheet. The effect of surface defects on C_{60} crystals was studied with GCMC simulations, and the difference in the results when compared with defect-free surfaces was explained on the basis of increased surface area.[16] Infrared spectroscopy of adsorbed CO on C_{60} crystals has indicated the existence of different adsorption sites,[17] which was later confirmed by GCMC simulations performed by Jiang et al.[18] While considerable work has been done to understand the adsorption properties of crystal phases of C_{60}, to our knowledge, there has been no study so far on the effect of the structural transformations on the surface characteristics of C_{70} crystals, and that was the purpose of this research.

Verheijen et al.[12] reported four crystal forms of C_{70}, a fcc phase at high temperature, rhombohedral (rh), deformed hexagonal-closed-packed (hcp I), ideal hexagonal-closed-packed (hcp II) phases near room temperature, and a monoclinic (mono) phase at low temperature. Tenedeloo et al.[13] have proposed the following route for phase transformations among the various crystal structures

$$\text{mono} \xleftrightarrow{\sim 276\ \text{K}} \text{hcp I} \xleftrightarrow{\sim 337\ \text{K}} \text{hcp II} \rightarrow \text{rh} \leftrightarrow \text{fcc}$$

These crystal phases primarily depend on the experimental conditions and synthesis route.[19] The structural data and orientational ordering of both high-temperature and low-temperature solid C_{70} had been studied extensively through X-ray diffraction,[11,13,20,21] electron diffraction,[13] electron microscopy,[11,13] constant-pressure molecular dynamics,[22] and optimal intermolecular potential-energy calculations.[23,24] In this work, we report how the surface properties of the C_{70} crystal change along the path of phase transformations. This is achieved by following a hierarchical approach; first, a quantum mechanical based potential for N_2-C_{70} interaction is determined and subsequently used in GCMC simulations. Predictions from a previously reported empirical potential and the ab initio based potential are compared by studying N_2 adsorption on the C_{70} fcc crystal phase. Then the BET surface area, monolayer capacity, and isosteric heat of adsorption of various C_{70} crystal phases are reported.

The outline of this paper is as follows. The following section is divided into two parts. First, the ab initio method used to obtain N_2-C_{70} interaction energies is explained along with the potential model used to fit these energies. In the second part, the simulation parameters for GCMC simulations are described, along with the lattice constants and corresponding orientational ordering of the C_{70} crystals. The results and discussion of quantum chemical calculations and GCMC simulations are

* Corresponding author. E-mail: sandler@che.udel.edu. Telephone: (302)-831-2945. Fax: (302)-831-3226.
[†] University of Delaware.
[‡] National Institutes of Health.

10.1021/jp050590t CCC: $30.25
Published on Web 08/18/2005

presented in Section III. Finally, the findings of this work are summarized and discussed in section IV.

II. Methods and Simulation Model

a. Ab initio Calculations. The quality of results from molecular simulations depends on the accuracy of the potential model used to describe molecular interactions. Bojan and Steele[25] developed a force field commonly used to model interactions of N_2 and O_2 separately with carbon surfaces by fitting low-coverage adsorption data on planar graphite sheets; we refer to this potential as the Steele potential. However, C_{70} is an ellipsoidal molecule with D_{5h} symmetry[26] and contains five- and six-membered carbon rings; in contrast, the graphite sheet is planar with symmetrically arranged hexagon rings. Also, C_{70} has five types of nonequivalent carbon atoms with the ratio 10:10:10:20:20, and there are eight distinct bond lengths among these atoms ranging from 1.38−1.47 Å.[27]

The Steele potential ignores the difference in the electronic structure between a flat graphite sheet and a curved surface of C_{70} fullerene. Moreover, apart from the curvature, the presence of five-membered carbon rings in C_{70} is also expected to result in changes in the electronic configuration. Therefore, as a first step in this work, we obtained an ab initio based potential between N_2 and C_{70} that incorporates these effects. For this, we used the recently developed hybrid method for calculating interaction energies (HM-IE).[28] HM-IE provides an accurate estimate of interaction energies calculated at a high level of theory (CCSD(T)) with a large basis set, but requires considerably less computational time.

The primary assumption in HM-IE is that the effects of electron correlation and basis set are additive, i.e., lower level theories (MP2 and MP4(SDQ)) can be used with large basis sets. The interaction energies calculated with HM-IE for neon, acetylene dimers, and the nitrogen−benzene system were in excellent agreement with the CCSD(T) energies and a large basis set (LBS).[28] For gases interacting with a carbon surface larger than benzene, the two-step HM-IE method was used to estimate the CCSD(T)/LBS energies,

$$\begin{aligned} E^{\text{int}}[\text{CCSD(T)/LBS}] \cong\ & E^{\text{int}}[\text{CCSD(T)/SBS}] + \\ & (E^{\text{int}}[\text{MP4(SDQ)/MBS}] - E^{\text{int}}[\text{MP4(SDQ)/SBS}]) + \\ & (E^{\text{int}}[\text{MP2/LBS}] - E^{\text{int}}[\text{MP2/MBS}]) \equiv E^{\text{int}}[\text{MP2}-4\text{:CC}] \end{aligned} \tag{1}$$

where MBS and SBS are a medium-sized basis set and a small-sized basis set, respectively. Consequently, high-level energy calculations are performed with small basis sets, and methods with less electron correlation are performed with medium- and large-sized basis sets. The basis set superposition error in all the interaction energy calculations was reduced or removed using the counterpoise correction method of Boys and Bernardi.[29] All the quantum mechanical calculations were performed using the Gaussian 98 suite of programs.[30]

For planar graphite sheets, the experimental adsorption data was fit to an atom site Lennard−Jones (LJ) 6−12 type potential. For the purpose of direct comparison, we also used this potential form to fit interaction energies obtained using the HM-IE method to obtain the force field for N_2−C_{70} interactions, although a different form could have been used[31,32]

$$\phi_{\text{LJ}}(r_{ij}) = 4\epsilon_{ij}\left[\left(\frac{\sigma_{ij}}{r_{ij}}\right)^{12} - \left(\frac{\sigma_{ij}}{r_{ij}}\right)^{6}\right] \tag{2}$$

where r_{ij} is the separation distance between sites i and j, σ_{ij} is the site collision diameter, and ϵ_{ij} is the well depth. Interactions including the quadrupole moment of nitrogen were found to have no significant effect on the adsorption results in graphite slit pores[33] and, recently, on the adsorption properties of N_2 on the curved surface of C_{168} schwarzite.[34] Therefore, quadrupole interactions were not accounted for in this work.

b. GCMC Simulations. GCMC simulations provide an effective way to study gas adsorption for various nanostructures.[35,36] In GCMC (constant adsorbate chemical potential, μ, volume, V, and temperature, T) simulations, the chemical potential of the adsorbed phase and bulk phase is kept in thermodynamic equilibrium by allowing the number of adsorbate molecules to fluctuate (creation and destruction of molecules). In addition to these two simulation moves, local equilibrium in the adsorbed phase is maintained by the additional moves of translating and rotating the adsorbed molecules.[37,38]

All GCMC simulations were performed at a temperature of 77.4 K (the normal boiling point of nitrogen). The system was first equilibrated for 4×10^6 moves, followed by a sampling period of 10^7 sample moves. The statistical error in the simulations was obtained by using the block transformation technique[38] with a sampling period divided into five equal blocks of 2×10^6 moves each. Periodic boundary conditions were used in the x and y directions, with the potential truncated at $5\sigma_{\text{N-C}}$ (16.8 Å) without any long-range corrections. Nitrogen was allowed to adsorb on the C_{70} crystal surface, which was kept perpendicular to the z-axis. A hard reflecting wall was kept parallel to the surface plane at a distance ranging from 15 to 50 Å, the shorter distance being for the low loading region to reduce the simulation time. The location of the wall was determined by varying its distance from the surface until there was no effect on the adsorbed molecules. Once equilibrium was reached, gas density was found to be almost negligible away from the surface (near reflecting wall), and therefore, all molecules in the course of simulations were considered to be adsorbed on the surface.

The system comprised of C_{70} molecules located at the lattice points of fcc, hcp, rhombohedral, and monoclinic crystal lattices, the parameters of which had been obtained by Oh and Lee.[24] They obtained these parameters, along with the orientational ordering of C_{70} molecules at the lattice points, by varying these constants in the ground-state structures of C_{70} crystal phases and minimizing energies. These constants were in good agreement with the experiment and were used for all the structures in this work. Figure 1 shows the orientation of C_{70} molecules in the various lattices. More details on the orientational ordering of these crystals can be found elsewhere.[24] The red semitransparent plane in Figure 1 depicts the plane along which N_2 was allowed to adsorb, namely (001) for the fcc and mono phases, and $(10\bar{1}0)$ for the hcp I, hcp II, and rh phases. All graphics in Figure 1 were plotted using VMD.[39]

The isosteric heat of adsorption provides a good measure to compare surface heterogeneity of different crystal structures and is more sensitive than the adsorption isotherms. In the limit of zero coverage, when adsorbent−adsorbent interactions are absent, this describes the affinity between the adsorbent and the crystal surface. The isosteric heat is then calculated using the following equation

$$q_{\text{st}} = (\underline{H}^{\text{b}} - \underline{H}^{*,\text{b}}) + RT - \left(\frac{\partial U^{\text{a,c}}}{\partial N^{\text{a}}}\right)_{T,V^{\text{a}}} \tag{3}$$

A detailed derivation of the above expression, along with the nomenclature used, is given in the Appendix. For ideal gas

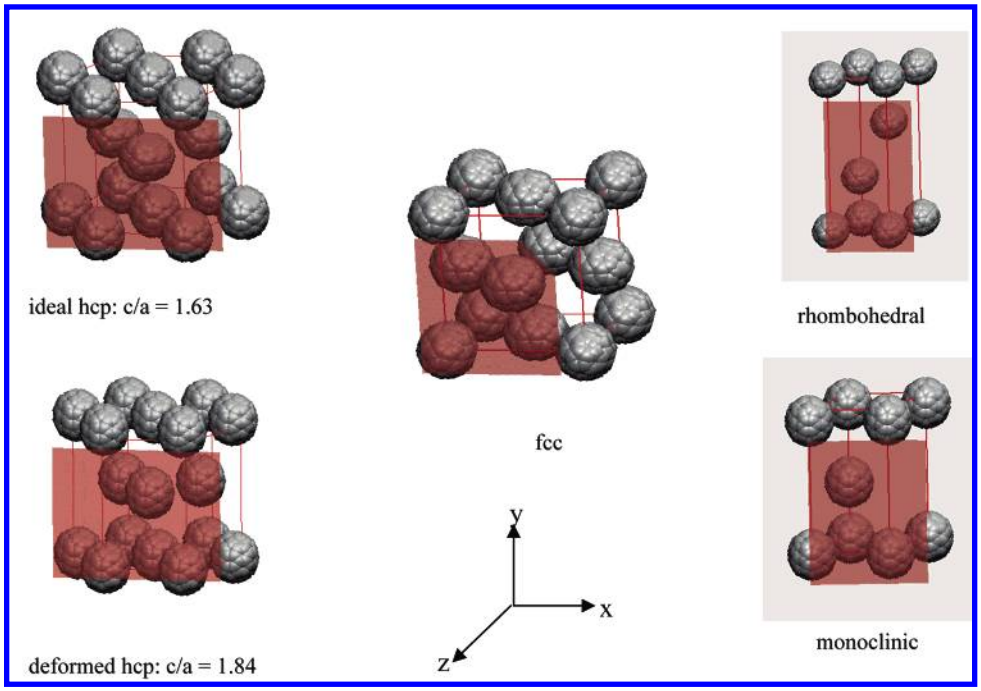

Figure 1. Orientational ordering of C_{70} in various crystal phases as obtained by Oh and Lee.[24] Semitransparent red plane represents the plane along which N_2 was adsorbed in the simulations.

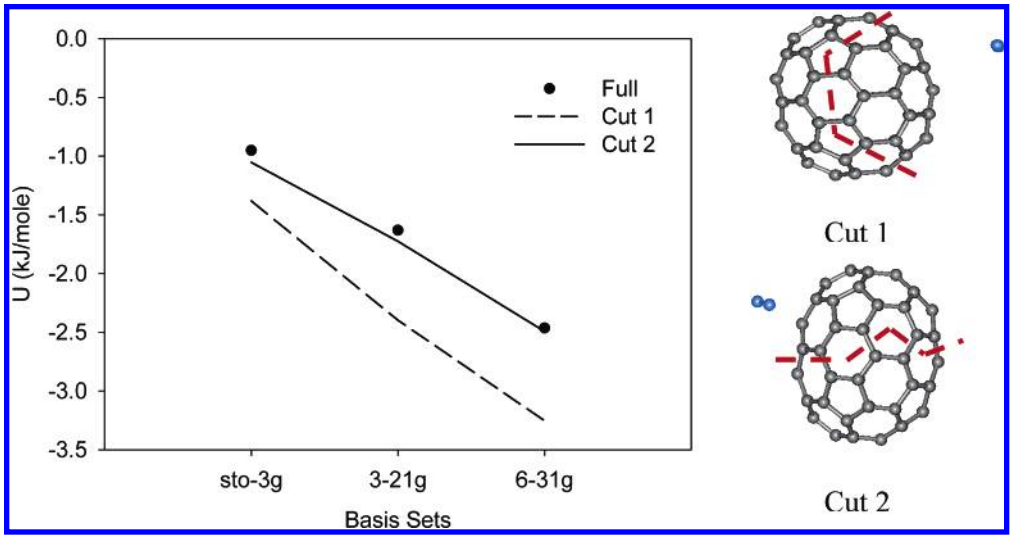

Figure 2. N_2-C_{70} MP2 interaction energies as a function of basis sets for the intact C_{70} molecule and two different cuts.

behavior in the bulk, eq 3 reduces to

$$q_{st} = RT - \left(\frac{\partial U^{a,c}}{\partial N^a}\right)_{T,V^a} \tag{4}$$

where $(\partial U^{a,c}/\partial N^a)_{T,V^a}$ can be obtained either by direct numerical differentiation of the configurational internal energy or by using fluctuation theory:

$$\left(\frac{\partial U^{a,c}}{\partial N^a}\right)_{T,V^a} = \frac{\langle UN\rangle - \langle U\rangle\langle N\rangle}{\langle N^2\rangle - \langle N\rangle^2} = \frac{f(U,N)}{f(N,N)} \tag{5}$$

We used both methods to calculate isosteric heats and thereby check for their consistency over the entire range of loading.

III. Results

a. Ab Initio Based Potential. Although HM-IE requires less computational time than CCSD(T)/LBS, calculations on a 70-carbon system involves more computational resources than what is currently available. Therefore, we used a method developed by Klauda and Sandler in their gas hydrate work[40] and also previously used to obtain potential parameters for N_2 and O_2 interactions with C_{168} schwarzite[36] and C_{60} fullerene.[18] Similar to those studies, the C_{70} molecule was first cut into two pieces of 34 and 36 carbon atoms to allow energy calculation with sufficient-sized basis sets. This required breaking of covalent bonds and these cleaved bonds were terminated with hydrogen atoms. Then, energies calculated at the MP2 level of theory at various basis sets for these cuts were used to determine the appropriate sized LBS in our HM-IE calculations. The N_2 interaction energy was calculated using the same orientation with respect to two different cuts of C_{70} and was found to be dependent on the nature of the cut as seen in Figure 2. Interaction energies of N_2 calculated using cut 2, which avoided cleavage of the five-membered carbon rings, resulted in good agreement with the calculation for the full C_{70}. Therefore, similar to previous graphite, C_{168}, and C_{60} calculations,[18,32,36] the 34-

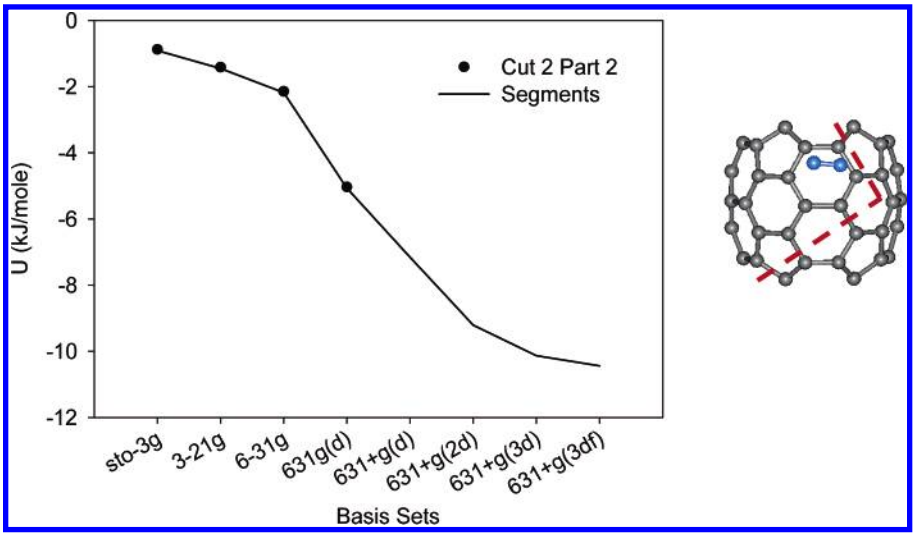

Figure 3. N_2 MP2 interaction energies as a function of basis set with intact 34-C atom cut and the sum of interaction energies with 18-C and 16-C segments.

TABLE 1: Lennard−Jones Potential Parameters for Nitrogen (N) and Carbon (C)

		C−N	
	N−N	Steele	QM
σ (Å)	3.32	3.36	3.358
ϵ/k_B (K)	36.4	33.4	37.968
l (Å)	1.10		

carbon piece was then used to calculate N_2 interaction energies with carbon in C_{70}.

The number of carbon atoms in the 34-carbon piece is too large to allow energy calculations with a sufficiently large sized basis set in a reasonable amount of computational time. Therefore, the 34 atom piece was further divided into two segments of 18 and 16 carbon atoms. As shown in Figure 3, good agreement was obtained between the interaction energy of the nitrogen molecule and the C_{70} section calculated using the sum of the two segments and with the intact cut piece of 34 carbon atoms. Similar to the results shown in Figure 2, calculations at all basis sets in Figure 3 were performed at the MP2 level of theory.

After determining the cuts and segments that properly represented the full C_{70} molecule, the two-step HM-IE approach (eq 1) was used to accurately calculate the interaction energies. There was only a small energy change in going from the 6-31+g(3d) basis set to 6-31+g(3df) (Figure 2), and therefore, the former provided a reasonable compromise between the accuracy and computational resources required, and was used as the LBS in our HM-IE calculations. As used by Klauda et al.[32] for C_{60} and C_{168}, the 6-31g(d) and 3-21g* basis sets were used for the MBS and SBS, respectively. HM-IE calculations were performed at 7 points, one in the repulsive region, two near the crossover region, one in the long-range attractive region, and three near the minima. Each point required an average of 29 days of computational time on a single AMD MP 1800+ processor.

The calculated nitrogen−carbon surface interaction energies ranged from −6.4 to 6.6 kJ/mol. These results were fit to atom site LJ 6−12 potential (eq 2), and the parameter values obtained are given in Table 1, along with Steele's potential for a planar graphite sheet. The ab initio based potential has a very similar collision diameter to that for the planar graphite sheet, but is more attractive, as was the case for C_{168} and C_{60}.[32] The results of the LJ fit to the HM-IE calculations along with the predictions

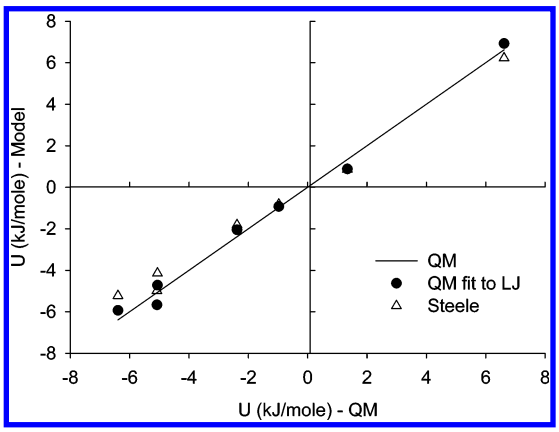

Figure 4. Goodness-of-fit test for the N_2-C_{70} interaction energies with ab initio based potential and the empirical Steele potential.

of interaction energies from Steele potential are shown in Figure 4. Because of a different well depth, ϵ_{N-C}, and similar size parameter, σ_{N-C}, the two potentials differ most near the potential minima, and are very similar in the long-range attractive, repulsive, and near-the-crossover regions.

The force field obtained here, though fit to a LJ 6−12 potential, incorporates the effect of carbon curvature and the presence of five-membered carbon rings on the electronic configuration, along with the contributions from all electrostatic interactions. This force field was then used for all the GCMC simulations of nitrogen adsorption on known C_{70} crystal surfaces.

b. GCMC Simulations. First, we compared the results obtained from ab initio potential and Steele's potential by performing GCMC simulations for nitrogen on the C_{70} fcc crystal at 77.4 K. As shown in Figure 5, the adsorption isotherms obtained from the two potentials were not very different at moderate and high pressure. However, at low pressure, there is a difference in the adsorption behavior between these two potentials, as was the case for adsorption isotherms on different crystal structures that will be discussed later.

Figure 6 shows the isosteric heat of adsorption at the infinite dilution and finite loadings obtained from both fluctuation theory and numerical differentiation of the internal configurational energy of the adsorbed molecules. The results obtained by these two methods were found to be consistent at all loadings. However, there was a moderate difference in the isosteric heat

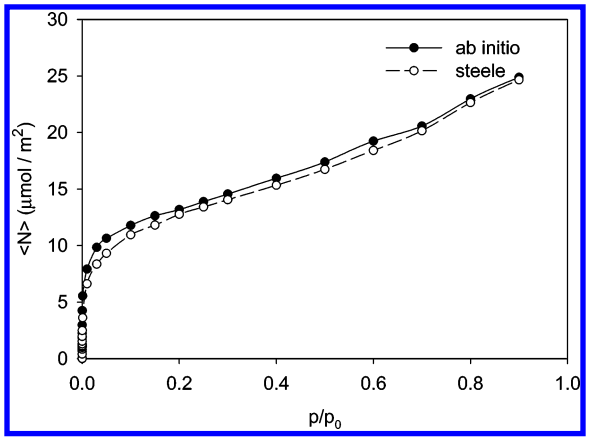

Figure 5. Adsorption isotherms of N_2 on C_{70} fcc crystal at 77.4 K. Adsorption coverage $\langle N \rangle$ is normalized by crystal surface area determined from BET equations.

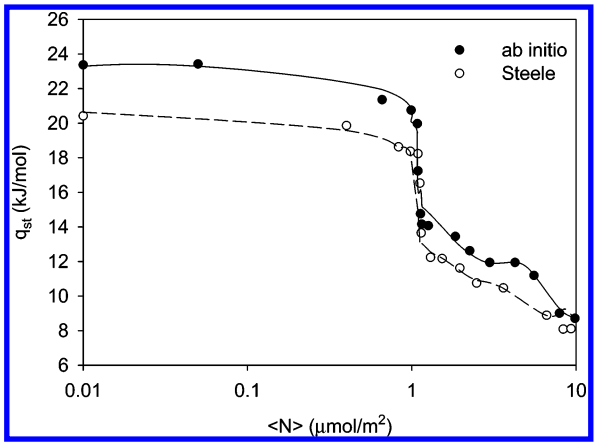

Figure 6. Isosteric heat of adsorption of N_2 on C_{70} fcc crystal at 77.4 K as a function of loading. Points marked with symbols are obtained from fluctuation theory and solid, dashed curves are obtained from numerical differentiation of the configurational internal energy.

of adsorption at finite loadings calculated using the two potentials. Isosteric heats calculated from the ab initio based potential were found to be consistently higher than those calculated from Steele's potential over the entire range of loading. This difference is highest in the infinite dilution limit (q_{st}^0), with 23.4 kJ/mol obtained using the ab initio based potential, while 20.42 kJ/mol was obtained from Steele's potential. The variation in the nitrogen−carbon potential is more evident in this dilute limit where N−C interactions dominate and N−N interactions are unimportant. The ab initio based potential, being more attractive than the planar graphite potential, leads to predictions of a higher q_{st}^0. For reference, q_{st}^0 for nitrogen adsorption on C_{60} fcc crystal is 23.1 and 20.3 kJ/mol from the ab initio based and Steele potential,[18] respectively, while on planar graphite sheets, q_{st}^0 has a much lower value of 10.1 kJ/mol.[41] These results suggest that the affinity for nitrogen on C_{60} (lattice constant = 14.17 Å) and C_{70} (lattice constant = 15.2 Å) fcc crystal surfaces is very similar while being considerably higher than that for planar graphite sheets. The heterogeneous surfaces of the C_{60} and C_{70} fcc crystals have strongly attractive octahedral sites, which are energetically very favorable for nitrogen adsorption, resulting in the large value of q_{st}^0. The filling of these sites then results in the drop in the isosteric heats seen in Figure 6.

The adsorption isotherms of nitrogen at 77.4 K on different C_{70} crystal structures are shown in Figure 7a. All isotherms are of Type II in the International Union of Pure and Applied

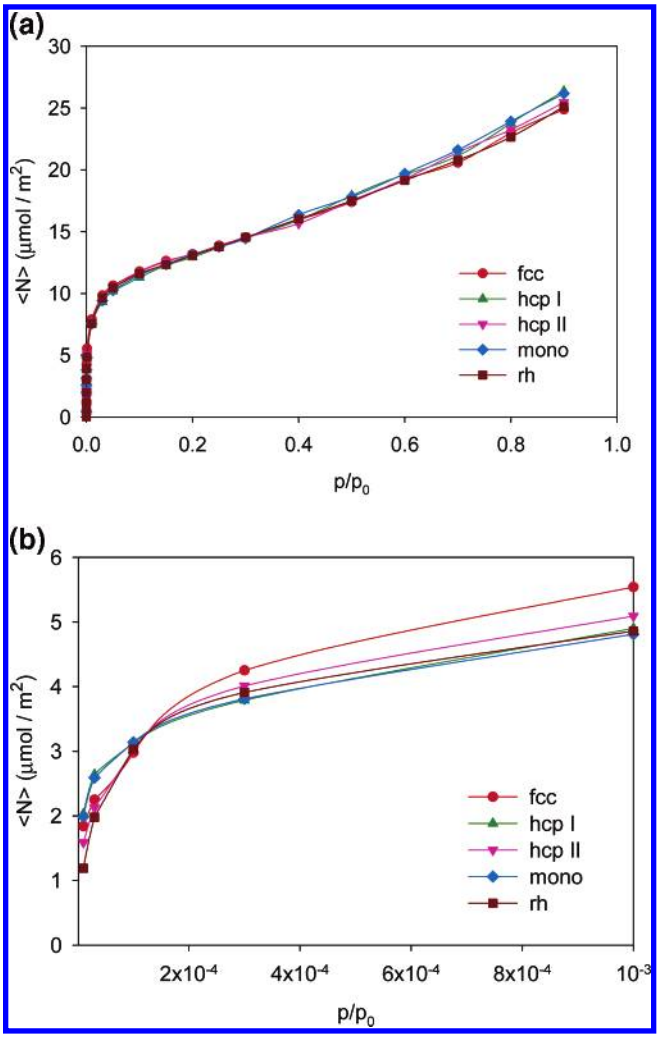

Figure 7. (a) Adsorption isotherms of N_2 on various C_{70} crystals at 77.4 K. Adsorption coverage $\langle N \rangle$ is normalized by crystal surface area determined from BET equations. (b) Same as in (a), but in the low-pressure range.

Chemistry (IUPAC) classification, which is a characteristic of adsorption on the surfaces of an adsorbent or within a macroporous material. Here, too, the adsorption isotherms are nearly identical for all the crystal phases at moderate and high pressures; however, there is a moderate difference in the adsorption behaviors at the low pressure where nitrogen−carbon interactions predominate (Figure 7b) and surface heterogeneity strongly affects the adsorption isotherms.

The isosteric heats of adsorption for all the crystals calculated using both fluctuation theory and numerical differentiation at a range of loading is shown in Figure 8. Again, results from both methods were found to be consistent for all crystals over the entire range of loading. The isosteric heats of adsorption are known to be more sensitive to the surface heterogeneity than the adsorption isotherms, and are often considered to be a signature of the surface topology. There is a considerable difference in the q_{st}^0 in the infinite dilution limit as shown in Figure 8. The face-centered cubic crystal was found to have the highest value of q_{st}^0 as a result of a stronger affinity for nitrogen.

Type II isotherms can be studied using the BET analysis to determine the surface area of adsorption, A_{BET}, and monolayer capacity, n_m.[42] In the form of a BET plot, the simulated adsorption isotherm data are linear in p/p_0 over the relative pressure range of 0.05 to 0.3 as shown in Figure 9. The solid

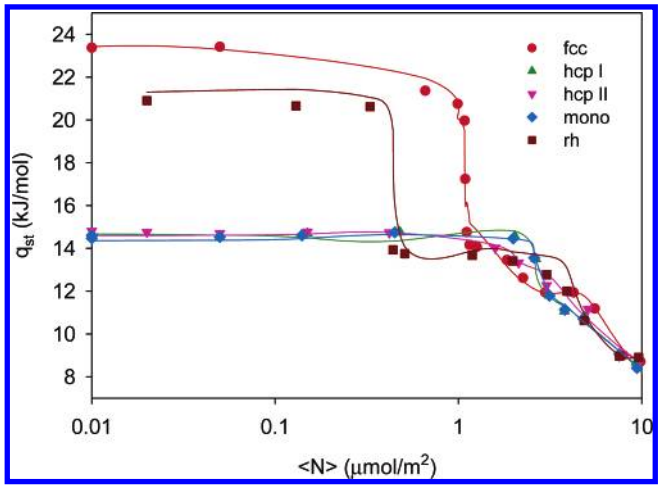

Figure 8. Isosteric heat of adsorption of N_2 on various C_{70} crystals at 77.4 K as a function of loading. Points marked with symbols are obtained from fluctuation theory, and solid curves are obtained from numerical differentiation of the configurational internal energy.

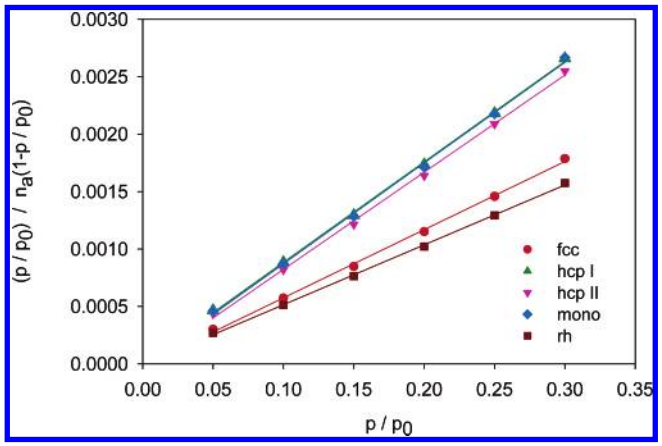

Figure 9. BET-coordinated plot of N_2 isotherms on various C_{70} crystals. Solid lines are obtained by regression of the adsorption isotherm points.

TABLE 2: Monolayer Capacity (n_m), BET Surface Area (A_{BET}), Isosteric Heats of Adsoption at Infinite Dilution (q_{st}^0) Obtained from N_2 Adsorption on C_{70} Crystal Surfaces

	n_m (μmol/m^2)	A_{BET}/A_{geom}	q_{st}^0 (kJ/mol)
monoclinic	12.46	1.22	14.5
hcp I	12.62	1.23	14.6
hcp II	12.91	1.25	14.7
rhombohedral	14.07	1.37	20.9
fcc	13.45	1.32	23.40 (ab initio) 20.42 (Steele)

lines in Figure 9 were obtained by linear regression of the data, and A_{BET} was calculated by using the N_2 cross-sectional area of 16.2 (Å)^2, standardized by IUPAC.

Tendeloo et al.[13] observed that the mono phase is formed by the orientational ordering transformation of hcp I phase. They also reported that, as hcp has abab layer packing, while rh and fcc phases have abcabc layer packing, the transformation from the hcp to the rh phase requires shear along the stacking of C_{70} molecules. These results were later explained by Oh and Lee[24] by calculating the binding energy curves for various orientational orderings of C_{70} crystals. Our results suggest that the rotational ordering of hcp to mono phase has a negligible effect on the surface heterogeneity with almost equivalent values for n_m, A_{BET}, and q_{st}^0 among the two phases (See Table 2). However, the shear transformation brings about a significant change in these properties, with q_{st}^0 showing a substantial drop between the rh and hcp II phases. Isosteric heats at infinite dilution were found to decrease along the path of phase transformation with the highest surface affinity for fcc crystal and lowest for the low-temperature mono phase. A moderate dependence of n_m and A_{BET} on the surface topology can also be seen in Table 2. The rh phase was found to have the largest surface area; however, the heterogeneous surface of fcc crystals had the highest affinity toward nitrogen in the monolayer regime as indicated by a higher value of q_{st}^0.

IV. Conclusions

We have developed a force field for the interaction of nitrogen with the C_{70} molecule that was found to be more attractive than the commonly used potential model of nitrogen interaction with a planar graphite sheet. The new force field is obtained using a recently developed method to accurately approximate the interaction energies from a high-level method with large basis sets. We have shown the importance of force fields in adsorption simulations, particularly in the low coverage region where nitrogen−carbon interactions are dominant. Isosteric heat of adsorption indicated that the C_{70} fcc crystal surface has a similar affinity for nitrogen as the C_{60} fcc crystal surface, with both being considerable higher than that of planar graphite sheets. Using atomistic simulations, we have simulated the dependence of the nitrogen adsorption properties on the C_{70} crystal surface topology as quantified by the monolayer capacity, BET surface area, and isosteric heat of adsorption in the limit of low coverage. We see that the shear-induced phase transformation has a greater effect on adsorption and the heterogeneity of the surface than the orientational ordering transformation.

Acknowledgment. This research was supported by grant number CTS-0083709 from the National Science Foundation and contract DE-FG02-85ER13436 from the Basic Energy Sciences Division of the U.S. Department of Energy. The authors are grateful to Drs. Jaeeon Chang and Jianwen Jiang for useful discussions.

Appendix

The isosteric heat of adsorption can be obtained experimentally by calorimetric calculations and corresponds to the differential entropy change when the fluid is transferred from the porous material to the bulk phase.

$$q_{st} = T\left[\left(\frac{\partial S^b}{\partial N^b}\right)_{T,P} - \left(\frac{\partial S^a}{\partial N^a}\right)_{T,V^a}\right] \tag{A1}$$

$$\left(\frac{\partial S^b}{\partial N^b}\right)_{T,P} = \frac{1}{T}\left[\left(\frac{\partial H^b}{\partial N^b}\right)_{T,P} - \mu^b\right] \tag{A2}$$

$$\left(\frac{\partial S^a}{\partial N^a}\right)_{T,V} = \frac{1}{T}\left[\left(\frac{\partial U^a}{\partial N^a}\right)_{T,V} - \mu^a\right] \tag{A3}$$

$$q_{st} = \left(\frac{\partial H^b}{\partial N^b}\right)_{T,P} - \left(\frac{\partial U^a}{\partial N^a}\right)_{T,V^a} = H^b - \left(\frac{\partial U^a}{\partial N^a}\right)_{T,V^a} \tag{A4}$$

The internal energy can be divided into a kinetic component U^k, and a configurational component U^c, the latter being absent

when the system is an ideal gas.

$$U = U^{k} + U^{c}$$

$$U^{k} = \frac{1}{2}RTs\langle N\rangle \tag{A5}$$

$$q_{st} = \underline{H}^{b} - \left(\frac{\partial U^{a,c}}{\partial N^{a}}\right)_{T,V^{a}} - \frac{s^{a}RT}{2} \tag{A6}$$

Assuming that there is no significant change in the internal degrees of freedom of fluid upon adsorption, the above expression reduces to

$$q_{st} = \underline{H}^{b} - \left(\frac{\partial U^{a,c}}{\partial N^{a}}\right)_{T,V^{a}} - \underline{H}^{*,b} + RT - RT \tag{A7}$$

$$q_{st} = (\underline{H}^{b} - \underline{H}^{*,b}) + RT - \left(\frac{\partial U^{a,c}}{\partial N^{a}}\right)_{T,V^{a}} \tag{A8}$$

Nomenclature

a = as superscript, adsorbed phase
b = as superscript, bulk phase
c = as superscript, configurational part
k = as superscript, kinetic part
i,*j*,*k* = as subscript, component indexes in mixture
* = as superscript, ideal behavior
0 = as superscript, infinite dilution property
− = as under bar, per mole property
μ = chemical potential
H = enthalpy
N = number of moles
R = gas constant
S = entropy
s = number of degrees of freedom
T = temperature
U = internal energy
V = volume
q_{st} = isosteric heat of adsorption

References and Notes

(1) Kratschmer, W.; Lamb, L. D.; Fostiropoulos, K.; Huffman, D. R. *Nature* **1990**, *347*, 354−358.
(2) Kratschmer, W.; Fostiropoulos, K.; Huffman, D. R. *Chem. Phys. Lett.* **1990**, *170*, 167−170.
(3) Baker, J.; Fowler, P. W.; Lazzeretti, P.; Malagoli, M.; Zanasi, R. *Chem. Phys. Lett.* **1991**, *184*, 182−186.
(4) Fowler, P. W.; Lazzeretti, P.; Malagoli, M.; Zanasi, R. *Chem. Phys. Lett.* **1991**, *179*, 174−180.
(5) Jensen, A. W.; Wilson, S. R.; Schuster, D. I. *Bioorg. Med. Chem.* **1996**, *4*, 767−779.
(6) Wang, Y. *Nature* **1992**, *356*, 585−587.
(7) Wang, Y.; West, R.; Yuan, C. H. *J. Am. Chem. Soc.* **1993**, *115*, 3844−3845.
(8) Higuchi, A.; Agatsuma, T.; Uemiya, S.; Kojima, T.; Mizoguchi, K.; Pinnau, I.; Nagai, K.; Freeman, B. D. *J. Appl. Polym. Sci.* **2000**, *77*, 529−537.
(9) Heiney, P. A.; Fischer, J. E.; McGhie, A. R.; Romanow, W. J.; Denenstein, A. M.; McCauley, J. P.; Smith, A. B.; Cox, D. E. *Phys. Rev. Lett.* **1991**, *66*, 2911−2914.
(10) David, W. I. F.; Ibberson, R. M.; Matthewman, J. C.; Prassides, K.; Dennis, T. J. S.; Hare, J. P.; Kroto, H. W.; Taylor, R.; Walton, D. R. M. *Nature* **1991**, *353*, 147−149.
(11) Vaughan, G. B. M.; Heiney, P. A.; Fischer, J. E.; Luzzi, D. E.; Rickettsfoot, D. A.; McGhie, A. R.; Hui, Y. W.; Smith, A. L.; Cox, D. E.; Romanow, W. J.; Allen, B. H.; Coustel, N.; McCauley, J. P.; Smith, A. B. *Science* **1991**, *254*, 1350−1353.
(12) Verheijen, M. A.; Meekes, H.; Meijer, G.; Bennema, P.; Deboer, J. L.; Vansmaalen, S.; Vantendeloo, G.; Amelinckx, S.; Muto, S.; Vanlanduyt, J. *Chem. Phys.* **1992**, *166*, 287−297.
(13) Vantendeloo, G.; Amelinckx, S.; Deboer, J. L.; Vansmaalen, S.; Verheijen, M. A.; Meekes, H.; Meijer, G. *Europhys. Lett.* **1993**, *21*, 329−334.
(14) Gusev, V. Y.; Ruetsch, S.; Popeko, L. A.; Popeko, I. E. *J. Phys. Chem. B* **1999**, *103*, 6498−6503.
(15) Martinez-Alonso, A.; Tascon, J. M. D.; Bottani, E. J. *Langmuir* **2000**, *16*, 1343−1348.
(16) Tascon, J. M. D.; Bottani, E. J. *J. Phys. Chem. B* **2002**, *106*, 9522−9527.
(17) Folman, M.; Fastow, M.; Kozirovski, Y. *Langmuir* **1997**, *13*, 1118−1122.
(18) Jiang, J.; Klauda, J. B.; Sandler, S. I. *J. Phys. Chem. B* **2005**, *109*, 4731−4737.
(19) Isakina, A. P.; Prokhvatilov, A. I.; Strzhemechny, M. A.; Yagotintsev, K. A. *Low Temp. Phys.* **2001**, *27*, 1037−1047.
(20) Valsakumar, M. C.; Subramanian, N.; Yousuf, M.; Sahu, P. C.; Hariharan, Y.; Bharathi, A.; Sastry, V. S.; Janaki, J.; Rao, G. V. N.; Radhakrishnan, T. S.; Sundar, C. S. *Pramana* **1993**, *40*, L137−L144.
(21) Janaki, J.; Rao, G. V. N.; Sastry, V. S.; Hariharan, Y.; Radhakrishnan, T. S.; Sundar, C. S.; Bharati, A.; Valsakumar, M. C.; Subramanian, N. *Solid State Commun.* **1995**, *94*, 37−40.
(22) Sprik, M.; Cheng, A. L.; Klein, M. L. *Phys. Rev. Lett.* **1992**, *69*, 1660−1663.
(23) Ghosh, G.; Sastry, V. S.; Radhakrishnan, T. S. *Phys. Rev. B* **1998**, *57*, R13969−R13972.
(24) Oh, D. H.; Lee, Y. H. *Phys. Rev. Lett.* **1995**, *75*, 4230−4233.
(25) Bojan, M. J.; Steele, W. A. *Langmuir* **1987**, *3*, 1123−1127.
(26) McKenzie, D. R.; Davis, C. A.; Cockayne, D. J. H.; Muller, D. A.; Vassallo, A. M. *Nature* **1992**, *355*, 622−624.
(27) Wang, C. Z.; Chan, C. T.; Ho, K. M. *Phys. Rev. B* **1992**, *46*, 9761−9767.
(28) Klauda, J. B.; Garrison, S. L.; Jiang, J. W.; Arora, G.; Sandler, S. I. *J. Phys. Chem. A* **2004**, *108*, 107−112.
(29) Boys, S. F.; Bernardi, F. *Mol. Phys.* **1970**, *19*, 553.
(30) Frisch, M. J.; Trucks, G. W.; Schlegel, H. B.; Scuseria, G. E.; Robb, M. A.; Cheeseman, J. R.; Zakrzewski, V. G.; Montgomery, J. A., Jr.; Stratmann, R. E.; Burant, J. C.; Dapprich, S.; Millam, J. M.; Daniels, A. D.; Kudin, K. N.; Strain, M. C.; Farkas, O.; Tomasi, J.; Barone, V.; Cossi, M.; Cammi, R.; Mennucci, B.; Pomelli, C.; Adamo, C.; Clifford, S.; Ochterski, J.; Petersson, G. A.; Ayala, P. Y.; Cui, Q.; Morokuma, K.; Malick, D. K.; Rabuck, A. D.; Raghavachari, K.; Foresman, J. B.; Cioslowski, J.; Ortiz, J. V.; Stefanov, B. B.; Liu, G.; Liashenko, A.; Piskorz, P.; Komaromi, I.; Gomperts, R.; Martin, R. L.; Fox, D. J.; Keith, T.; Al-Laham, M. A.; Peng, C. Y.; Nanayakkara, A.; Gonzalez, C.; Challacombe, M.; Gill, P. M. W.; Johnson, B. G.; Chen, W.; Wong, M. W.; Andres, J. L.; Head-Gordon, M.; Replogle, E. S.; Pople, J. A. *Gaussian 98*, revision A.9; Gaussian, Inc.: Pittsburgh, PA, 1998.
(31) Klauda, J. B.; Jiang, J. W.; Sandler, S. I. *J. Phys. Chem. B* **2004**, *108*, 9842−9851.
(32) Klauda, J. B.; Jiang, J.; Sandler, S. I. *J. Phys. Chem. B* **2004**, *108*, 9842−9851.
(33) Kaneko, K.; Cracknell, R. F.; Nicholson, D. *Langmuir* **1994**, *10*, 4606−4609.
(34) Jiang, J. W.; Sandler, S. I., *J. Am. Chem. Soc.* **2005**, submitted.
(35) Arora, G.; Wagner, N. J.; Sandler, S. I. *Langmuir* **2004**, *20*, 6266−6277.
(36) Jiang, J.; Klauda, J. B.; Sandler, S. I. *J. Phys. Chem. B* **2004**, *108*, 9852−9860.
(37) Frenkel, D.; Smit, B. *Understanding Molecular Simulation*; Academic Press: London, 1996.
(38) Allen, M. P.; Tildesley, D. J. *Computer Simulation of Liquids*; Oxford University Press: Oxford, 1987.
(39) Humphrey, W.; Dalke, A.; Schulten, K. *J. Mol. Graphics* **1996**, *14*, 33.
(40) Klauda, J. B.; Sandler, S. I. *J. Phys. Chem. B* **2002**, *106*, 5722−5732.
(41) Bojan, M. J.; Steele, W. A. *Langmuir* **1987**, *3*, 116−120.
(42) Branauer, S.; Emmett, P. H.; Teller, E. *J. Am. Chem. Soc.* **1938**, *60*, 309−319.